Supplementary Materials for

A Periciliary Brush Promotes the Lung Health by Separating the Mucus Layer from Airway Epithelia

Brian Button, Li-Heng Cai, Camille Ehre, Mehmet Kesimer, David B. Hill, John K. Sheehan, Richard C. Boucher, Michael Rubinstein*

*To whom correspondence should be addressed. E-mail: mr@unc.edu

Published 24 August 2012, *Science* **337**, 937 (2012)
DOI: 10.1126/science.123012

This PDF file includes:

Supplementary Materials for

A Periciliary Brush Promotes the Lung Health by Separating the Mucus Layer from Airway Epithelia

Brian Button[1†], Li-Heng Cai[2†], Camille Ehre[1], Mehmet Kesimer[1, 3], David B. Hill[1], John K. Sheehan[3], Richard C. Boucher[1‡], Michael Rubinstein[2, 4‡*]

[1]Cystic Fibrosis Research and Treatment Center, University of North Carolina, Chapel Hill, NC 27599-7248, USA.

[2]Curriculum in Applied Sciences and Engineering, University of North Carolina, Chapel Hill, NC 27599-3280, USA.

[3]Department of Biochemistry and Biophysics, University of North Carolina, Chapel Hill, NC 27599-7260, USA.

[4]Department of Chemistry, University of North Carolina, Chapel Hill, NC 27599-3290, USA.

*Correspondence to: mr@unc.edu
[†]The first two authors (Button and Cai) contributed equally to this work.
[‡] Rubinstein and Boucher are two senior authors.

This PDF file includes:

Materials and Methods

Both fluorescently-labeled and non-fluorescent dextran fractions with narrow molecular size distributions were obtained using size exclusion chromatography and their weight average hydrodynamic diameters (d) were characterized by dynamic light scattering. To image the penetration of dextran molecules into the PCL, a dilute mixture of green-fluorescent dextran of size d and small ($d \approx 2$ nm) Texas Red fluorescent dextran was added onto well-differentiated HBE cell cultures.

In experiments measuring the PCL collapse under osmotic compression, various concentrations of endogenous mucus or mucus simulants (large non-fluorescent dextran ($d > 50$ nm) and agarose ($d \approx 44$ nm)) were combined with the fluorescent-dextran mixture (large green ($d > 50$ nm) and small Texas Red). High resolution XZ-confocal images were obtained using a multi-laser scanning confocal microscope (Model SP5; Leica). Bright field microscope was used to measure the height of the cilia exposed to mucus/mucus simulants of various concentrations. The dependence of osmotic pressure of the endogenous mucus/mucus simulants on their concentration was measured using a custom-designed membrane osmometer (*47*) and then their osmotic moduli were calculated. In experiments measuring the osmotic pressure of endogenous mucus on HBE cells, excised culture membranes were positioned directly on the osmometer's membrane, in the absence of exogenous fluid (*37*).

Human tissue procurement and cell culture. Tissues and cells were provided by the Cystic Fibrosis (CF) Center Tissue Core Facility of the University of North Carolina at Chapel Hill under the auspices of protocols approved by the Institutional Committee on the

protection of the rights of human subjects. HBE cells from non-CF lungs are harvested by enzymatic digestion as previously described (*48*). Disaggregated human bronchial epithelial (HBE) cells are seeded on 12 mm diameter Transwell Clear supports (Corning Costar, Cambridge, MA) at a density of 2.5×10^5 cells/cm^2 in a well-defined airway cell media (*48*). Cultures are maintained at an air-liquid interface until fully differentiated (~ 4 weeks).

Transmission electron microscopy (TEM). Samples for electron microscopy were obtained from cryopreserved HBE cell cultures. Cryopreservation was used to maintain native conformation of mucus layer, periciliary layer (PCL), plasma membranes, and cilia. Cell sections were examined using a FEI/Phillips Tecnai 12 (FEI Company, Hillsboro, OR) TEM at 80 kV with a 1k×1k CCD camera (Gatan, Pleasanton, CA) to assess their structure at a submicron level.

Antibodies. Monoclonal antisera against MUC1 mucin was purchased from Fujirebio Diagnostics, Inc. (Japan), an antibody that recognizes a sialylated carbohydrate epitope expressed on the MUC1 mucin. Rabbit polyclonal antibody against MUC4 mucin was produced in our laboratory using a specific synthetic peptide located in the type D domain of von Willebrand factor (vWF-D) (*49*).

Immunohistochemistry. Human specimens were obtained postmortem from non-smoking patients. Intermediate-size airways were dissected and fixed in paraformaldehyde. Paraffin-embedded sections were dewaxed and hydrated. Antigens were retrieved by

Dako target retrieval solution (Dako Corporation, Carpinteria, CA). Sections were stained with 4', 6-diamidino-2-phenylindole (DAPI) for nuclei, with monoclonal or polyclonal antisera and revealed by anti-mouse or anti-rabbit Alexa-conjugated secondary antibodies. Images were captured using a Leica SP5 confocal microscope (Leica, Mannheim, Germany).

Fractionation of dextran (unlabeled and fluorescently labeled). Size exclusion chromatography was used to separate green fluorescently-labeled dextrans into fractions with well-defined molecular sizes (weight average hydrodynamic diameter *d*). Raw batches of 2 MDa dextran (purchased from Sigma-Aldrich, St. Louis, MO and Invitrogen, Carlsbad, CA) was fractionated by a Sepharose CL-2B column (GE Healthcare Life Sciences, Buckinghamshire, England) and eluted by phosphate buffered saline (PBS) with elution volume of 150 ml at a flow rate 0.2 ml/min using a Rheos 2000 pump (Flux Instruments, Basel, Switzerland). Fractions of 2 ml were collected and characterized by dynamic light scattering to obtain the hydrodynamic size of fractionated polymers. Fractionated dextran molecules with desired sizes were dialyzed (10 kDa molecular weight cutoff, Thermo Scientific, Rockford, IL) against distilled water and then lyophilized prior to use.

Osmotic pressure/moduli measurements. In these studies, we employed a custom-designed direct-membrane osmometer (*47*) equipped with a salt and small protein permeable osmotic membrane to measure the osmotic pressure of various mucus simulants (dextran and agarose) as well as of endogenous mucus. This device consists of

a fluid chamber connected to a sensitive pressure transducer (Omega Engineering, Stamford, CT) affixed to the bottom of the chamber. A 25 mm diameter polyethersulfone membrane (Millipore Inc., Bedford, MA) separated the test chamber from the reference chamber filled with PBS. The osmometer was calibrated with commercial osmotic pressure standards (Wescor Inc., Logan, UT).

An osmotic membrane with 10 kDa molecular weight cutoff (MWCO), which has pore diameter about 2.8 nm extrapolated from the data in ref. (*50*), was used for measuring the osmotic pressure of mucus simulants. In each measurement, 0.2 ml of the mucus simulant was placed into the fluid chamber, allowing it to come into contact with the pressure transducer. The steady-state osmotic pressure of a mucus simulant with a given concentration was recorded.

The above system was modified to measure the osmotic pressure of endogenous mucus accumulated on the surface of HBE cultures, using the approach for measuring oncotic pressures from excised tissue samples (*37*). Here, mucus was allowed to accumulate on the surface of the HBE epithelium for up to 4 weeks. The culture-insert membrane (Transwell-Clear; Corning Costar, Cambridge, MA) was carefully excised with a scalpel and placed directly onto a 100 kDa MWCO (pore diameter ~11 nm measured by solute transport methods (*50*)) osmotic membrane with the apical side facing down. To investigate the change in the osmotic pressure with mucus concentration, parallel cultures were exposed to various amounts of exogenous fluid (5–40 μl of PBS) approximately 1 hour before the osmotic pressure measurements. To measure the mucus concentration under each experimental condition, dry-to-wet ratio experiments were performed (*10*) in parallel cultures. The obtained concentration defined

as the ratio of total mass of solids in mucus to the mass of mucus, including the salt contribution (~1%), is conventionally called % solids. By subtracting 1% from this value one can convert % solids to the concentration in terms of g/ml, corresponding to the mass of solids excluding salts per unit volume of mucus, as the density of mucus is ~1 g/ml. For instance, 2% solids is equivalent to 0.01 g/ml.

In all experiments, the osmotic moduli of mucus simulants (dextran and agarose) and endogenous mucus were calculated from the concentration dependence of osmotic pressure using equations presented in **Supplementary Text**.

Measurements of the permeability of PCL using confocal microscopy. To image the penetration of dextran molecules of different sizes into the PCL, we employed a dual-labeling technique of the PCL layer. In each experiment, a solution of green-fluorescent probe dextran of a particular hydrodynamic diameter d was mixed with the solution of small ($d \approx 2$ nm) unfractionated Texas Red fluorescent dextran (average molecular weight 3 kDa). Dilute solution of this mixture was then added to the lumen of a freshly washed HBE culture. Both fluorescent reagents were added at a concentration of ~ 0.1 mg/ml in PBS (with osmotic pressure on the order of 1 Pa). In each experiment, 50 μl solutions were added to cell culture and studied within 30 minutes to ensure no significant effects of water absorption by cells. High resolution XZ-confocal images were obtained using a Leica TCS SP5 laser scanning confocal microscope. The exclusion thickness of the green dye was measured as the difference in the thickness of the red and yellow (red + green) regions (**Fig. 3B**).

Transmission-light imaging of cilia height. Images of the airway cilia before and after exposure to the various osmotic reagents were obtained using differential interference contrast (DIC) microscopy of sections of airway cultures viewed in profile. Here, 1mm ×12mm sections of HBE cell cultures were placed in a special chamber allowing access to the apical and basolateral solutions. After control images in PBS, the apical solution was replaced with the 150 μl desired osmotic reagents. A custom perfusion device was used to exchange solutions during these studies. For studies investigating the cilia height under various concentrations of endogenous mucus, immiscible perfluorocarbon (Fluorinert FC-77, 3M Specialty Materials, St. Paul, MN) was carefully placed on both the apical and basolateral compartments to prevent dehydration (*51*).

Supplementary Text

Osmotic modulus. The osmotic modulus K of a solution defined as

$$\mathrm{K} = c\frac{\partial \pi}{\partial c} \tag{S1}$$

describes the rate at which its osmotic pressure π changes with concentration c. Typically osmotic pressure of polymer solutions in a good solvent can be described by the crossover phenomenological equation (*32*)

$$\pi = \frac{N_{Av}k_BT}{M_n}c\left(1+\left(c/c^*\right)^{\alpha-1}\right) \tag{S2}$$

where N_{Av} is the Avogadro number, k_B is the Boltzmann constant, T is the absolute temperature, M_n corresponds to the number average molar mass of polymer, and c^* is the polymer overlap concentration. Therefore, the osmotic modulus K defined by eq. S1 is

$$\mathrm{K} = \frac{N_{Av}k_BT}{M_n}c\left(1+\alpha\left(c/c^*\right)^{\alpha-1}\right) \tag{S3}$$

Dextran. We have measured the osmotic pressure π of dextran solutions at concentrations ranging from dilute to semidilute regime, in which dextran molecules are overlapping with each other (*32*). The dependence of dextran osmotic pressure on solution concentration was fitted by eq. S1 (see thin solid red line in **fig. S1**):

$$\pi_{dex} = 1.2\times10^4\,\frac{\mathrm{Pa}}{\mathrm{g/ml}}\times c\left(1+\left(\frac{c}{0.025\,\mathrm{g/ml}}\right)^{1.25}\right) \tag{S4}$$

The value of exponent α= 2.25 is in perfect agreement with previous study (*52*). Equation S4 corresponds to the number average molar mass of dextran $M_n = 2\times10^5$ g/mole and the

overlap concentration c^* = 0.025 g /ml. The average molecular size $\left\langle R_g \right\rangle_n^{1/3}$ of polymers can be estimated from the number average molar mass and overlap concentration

$$c^* = \frac{M}{N_{Av}V} \approx \frac{\sum_i n_i M_i}{N_{Av}\sum_i n_i \left(R_g\right)_i^3} = \frac{M_n}{N_{Av}\left\langle R_g^3 \right\rangle_n} \tag{S5}$$

where M is the total molar mass of polymers in pervaded volume V, n_i is the number fraction of polymers with molar mass M_i, and $(R_g)_i$ is the corresponding radius of gyration. Therefore, the average molecular size of dextran molecules is

$$\left\langle R_g^3 \right\rangle_n^{1/3} \approx \frac{M_n}{c^* N_{Av}} \approx 24 \text{ nm} \tag{S6}$$

This average size of dextran molecules is consistent with the average molecular size obtained from both size exclusion chromatography and dynamic light scattering characterizations. From eq. S4 one can obtain the osmotic modulus K (eqs. S1 and S3) of dextran solutions (see thin dashed red line in the insert of **fig. S1**):

$$\mathrm{K}_{dex} = 1.2\times10^4 \frac{\text{Pa}}{\text{g/ml}} \times c\left(1 + 2.25\left(\frac{c}{0.025\ \text{g/ml}}\right)^{1.25}\right) \tag{S7}$$

This equation was used to estimate the osmotic modulus of dextran solutions in the PCL compression and collapse experiments.

Agarose. The concentration dependence of osmotic pressure of agarose in PBS solution was measured at 37 °C to keep low-melting point agarose from gelling (blue triangles in **fig. S1**). Fitting these data to eq. S2 we obtained the expression for concentration dependence of the agarose osmotic pressure (see the medium solid blue line in **fig. S1**)

$$\pi_{agr} = 3.6\times10^4 \frac{\text{Pa}}{\text{g/ml}} \times c\left(1+\left(\frac{c}{0.027\ \text{g/ml}}\right)^{1.25}\right) \quad \text{(S8)}$$

The linear (van't Hoff) term of agarose osmotic pressure is consistent with the number average molar mass of 7×10^4 g/mole and the overlap concentration leads to molecular size $\left\langle R_g \right\rangle_n^{1/3} \approx 16$ nm. This value is consistent with the average molecular size obtained from dynamic light scattering characterization. The osmotic modulus of agarose solution is calculated using eqs. S1 and S8

$$\mathrm{K}_{agr} = 3.6\times10^4 \frac{\text{Pa}}{\text{g/ml}} \times c\left(1+2.25\left(\frac{c}{0.027\ \text{g/ml}}\right)^{1.25}\right) \quad \text{(S9)}$$

and plotted by the medium dashed blue line in the insert of **fig. S1**. Equation S9 was used to estimate the osmotic modulus of agarose solution.

Mucus. The osmotic modulus of mucus was determined from the concentration dependence of mucus osmotic pressure. We observed two regimes of the concentration dependence of mucus osmotic pressure. Within the low concentration regime (from ~0.02 g/ml to ~0.06 g/ml), the osmotic pressure of mucus has a linear dependence on concentration $\pi\sim c$. In the high concentration regime (from ~0.08 g/ml to ~0.14 g/ml), the osmotic pressure increases as a higher power of concentration $\pi\sim c^{\beta}$, where $\beta=2.21\pm0.17$. Since there is a sharp crossover between these two dependencies, we used a modified crossover expression

$$\pi_{muc} = kc\left[1+\left(c/c^*\right)^{(\beta-1)m}\right]^{\frac{1}{m}} \quad \text{(S10)}$$

to fit the data over the whole concentration range, with crossover exponent m=3, coefficient k=(1.45±0.29)×10^4 Pa/(g/ml) and crossover concentration c^*=0.081±0.019 g/ml. The fit of the mucus osmotic pressure to eq. S10 is shown in **fig. S1** (thick solid green line).

Osmotic modulus (defined by eq. S1) of native mucus is calculated using eq. S10

$$\mathrm{K}_{muc} = 1.45\times10^4 \frac{\mathrm{Pa}}{\mathrm{g/ml}} \times c\left(1+\left(\frac{c}{0.081\,\mathrm{g/ml}}\right)^{3.63}\right)^{1/3}\left[1+\frac{1.21\times\left(\frac{c}{0.081\,\mathrm{g/ml}}\right)^{3.63}}{1+\left(\frac{c}{0.081\,\mathrm{g/ml}}\right)^{3.63}}\right] \qquad \text{(S11)}$$

and is depicted by the thick dashed green line in the insert in **fig. S1**. This expression of the osmotic modulus of mucus was used to construct the plot (**Figs. 4B, 5E**) of the dependence of PCL and cilia heights on mucus osmotic modulus.

PCL penetration analysis. The mesh size of PCL in living HBE cultures was determined from the measurements of the penetration depth into the PCL by fractionated fluorescently-labeled probe molecules (e.g. dextrans) of well-defined sizes following the addition of dilute solution of these probe molecules to the luminal side of HBE cultures. The results are reported as the dependence of penetration depth (distance from the epithelial cell surface) on the weight average hydrodynamic diameter of probe molecules. The penetration depth was measured as the average thickness of the red zone in the confocal images (see **Fig. 3B**).

Note that each fraction of probe molecules obtained by size exclusion chromatography is not perfectly monodisperse. The reported size corresponds to the weight average hydrodynamic diameter of each fraction. To rationalize this protocol we

compare the results obtained by using the weight average hydrodynamic diameter with the analysis that takes into account the actual distribution of dextran sizes (the "full profile analysis"). Below we demonstrate that the results obtained from these two methods are in reasonable agreement with each other within the error of our measurements.

The basic assumption of "full profile analysis" is that probe molecules can freely penetrate into the PCL down to a distance z from epithelial cell surface, at which the mesh size $\xi(z)$ in the PCL is on the order of the diameter d of probe molecules. If we denote the exclusion thickness z for probe molecules with hydrodynamic diameter d, the shortest distance of these molecules from the cell surface, by z_d, then we conclude that the mesh size at this distance: $\xi(z_d) \approx d$. This assumption approximates distribution profile of probe molecules with size d in the PCL by a step function: molecules with size d are evenly distributed in the region with mesh size larger than d, corresponding to the distance from the cell surface further than z_d; whereas they are excluded from the region with the distance from the cell surface closer than z_d, where the mesh size ξ is smaller than d.

Each fraction of dextran molecules was characterized by dynamic light scattering and a distribution of the scattered light intensity versus the logarithmic of hydrodynamic diameter ($\log[d]$) was obtained. Dividing the intensity value by the corresponding molecular size d one obtains the intensity distribution on linear molecular size scale: $I(d)$ vs. d, shown in **fig. S2A**. Note that the scattered light intensity is proportional to the product of concentration c and mass M of polymers: $I \sim cM$. Therefore, one can convert the intensity-size distribution $I(d)$ to the concentration-size distribution $c(d)$ via

$$c(d) \sim I(d)/M \sim I(d)/d^{1/\nu} \tag{S12}$$

because the mass M of polymers is proportional to the power of polymer size d: $M \sim d^{1/\nu}$, where ν is the Flory exponent in a good solvent. For flexible linear polymers $\nu \approx 3/5$ (*32*) and for randomly branched polymers $\nu \approx 1/2$ (*53, 54*). Dextran is a linear molecule at low molecular weights and a branched molecule at high molecular weights. In our analysis $\nu \approx 1/2$ was used for dextran fractions with molecular weight higher than 10 kDa (*52*) and $\nu \approx 3/5$ was used for 3 kDa Texas Red dextran.

A typical normalized concentration-size distribution $c(d)$ of a fraction of probe molecules is shown by the green solid line in **fig. S2B**. From this distribution one can 1) estimate the weight average hydrodynamic diameter as $\langle d \rangle_w \equiv \sum_i c_i d_i \Big/ \sum_i c_i$, in which c_i is the concentration for polymers with hydrodynamic diameter d_i; and 2) calculate the normalized concentration distribution $S(d)$ of molecules within this fraction that are smaller than d:

$$S(d) = \int_{d_{\min}}^{d} c(d)\mathrm{d}d \Big/ \int_{d_{\min}}^{d_{\max}} c(d)\mathrm{d}d \tag{S13}$$

shown by the solid green line in **fig. S2C**. This normalized concentration $S(d)$ corresponds to the weight fraction of molecules that are able to penetrate mesh of size $\xi \approx d$ and, therefore, is proportional to the fluorescent intensity of this fraction of probe molecules in the PCL.

We measured the fluorescent intensity (concentration) of probe molecules in the PCL as a function of distance from the cell surface. The normalized fluorescent intensity at distance z from the cell surface is denoted by $Q(z)$ and shown by the green plot in **fig. S2D**. The cell surface is determined by the lower bound of the penetration of small

(weight average hydrodynamic diameter $\langle d \rangle_w \sim$ 2 nm) red dextran molecules (see extrapolation of the red curve to $Q(z=0) = 0$ in **fig. S2D**, and **fig. S4**).

Our step function approximation implies that for the same values of the normalized distributions $S(d)$ and $Q(z)$, the hydrodynamic diameter d of probe molecules is related to the distance z from the cell surface at which the penetration of these molecules is stopped. This analysis allows one to obtain a profile $z(d)$ describing the dependence of exclusion thickness z on molecular size d for any solution of probe molecules with known size distribution.

The results on the exclusion profile $z(d)$ of probe molecules obtained by the above "step function profile analysis" of nine different fractions of green probe molecules are shown by green symbols in **fig. S2E**. These results can be described by a phenomenological equation

$$z(d) \approx z_0 \left[1 - \exp\left(-d/\bar{\xi}\right)\right], \quad \text{for } 0 < z < z_0 \tag{S14}$$

in which z_0=7.0±0.5 μm is the maximum height of the PCL and the characteristic PCL mesh size is $\bar{\xi}$ =17.5±2.4 nm (see the dashed line in **fig. S2E**). This equation describes the penetration profile of probe molecules with different sizes into the PCL. The penetration profile obtained using the weight average molecular size as reported value is shown by solid squares in **fig. S2E** and the best fit to this profile is presented by the solid line (eq. S14) with z_0=6.9±0.8 μm and $\bar{\xi}$ =15.0±3.7 nm. These results indicate that the penetration profile obtained using the weight average molecular size is in agreement with that using "step function profile analysis" within the error of our measurements.

In the above we assumed that probe molecules of a particular size d in each fraction follow a "step function" distribution in the PCL. In fact, probe molecules with

size d can penetrate into the PCL to a distance z from the cell surface smaller than z_d, at which the mesh size $\xi(z<z_d)$ is smaller than diameter d, but they have to pay free energy penalty on the order of $k_BT(d/\xi(z))^{\gamma}$ (*55*). Here the exponent γ depends on the type of the probes and solvent quality. For a solid probe particle γ=3, for a linear flexible polymer γ=5/3 in a good solvent and γ=2 in a theta solvent (*32*), and for a randomly branched polymer γ=2 in a good solvent (*54*) and γ=16/7 in a theta solvent (*53*). Therefore, the distribution $P(z)$ of probe molecules with size d in the PCL at distance z smaller than z_d becomes

$$P(z) = \text{const} \times \exp\left[-\left(d/\xi(z)\right)^{\gamma}\right], \quad \text{for } z < z_d \tag{S15}$$

The results obtained from "profile analysis" by considering dextran as a randomly branched polymer in a good solvent (γ=2) (*52*) are shown by the blue symbols in **fig. S2F**. The best fit of eq. S14 to these data is shown by the blue dash-dotted line with z_0=6.9±0.4 μm and $\bar{\xi}$ =15.0±2.0 nm, which is in good agreement with the results of analysis using the "step function" approximation, shown by the green symbols and the green dashed line in **fig. S2F**. Furthermore, considering dextran as a solid particle (γ=3) leads to almost identical results (z_0=6.9±0.4 μm and $\bar{\xi}$ =15.8±2.1 nm; red symbols and red solid line in **fig. S2F**). The fitting parameters z_0 and $\bar{\xi}$ of eq. S14 to the results from different types of analysis are listed in **table S1**. As clear from **table S1**, all methods of profile analysis agree with each other within experimental error bars.

Mesh size distribution in the periciliary layer. As illustrated in **fig. S3A**, the PCL is modeled as an array of cylindrical brushes, in which each brush consists of a cylindrical

core (cilium) and grafted polymers (tethered macromolecules), shown in **fig. S3B**. A single cilium brush in an unperturbed state is shown in **fig. S3C**, in which R_{cilium} is the radius of the cylinder (cilium) and the thickness L_0 is defined as the average distance from the center of the cylinder to the free ends of tethered macromolecules. The mesh size (correlation length) $\xi(r)$ in an unperturbed cylindrical brush at distance r from the center of the cylinder is related to the grafting density σ of the macromolecules to the surface of the cilium as (*56*)

$$c(d) \sim I(d)/M \sim I(d)/d^{1/\nu} \tag{S16}$$

which is shown by **fig. S3C** and the dashed line in **fig. S3E**. The volume fraction profile of tethered macromolecules is

$$\xi(r) \approx \left(\xi(r)/b\right)^{(1-3\nu)/\nu}, \quad \text{for } r > R_{cilium} \tag{S17}$$

where ν is Flory exponent depending on solvent quality (for a theta solvent $\nu=1/2$ and for a good/athermal solvent $\nu=3/5$) (*32*) and b corresponds to the Kuhn length of polymers. Here $\nu=3/5$ is used as the physiological solutions are good solvent for macromolecules like mucins. The volume fraction profile (eq. S17) can be rewritten in terms of the distance r from the center of the cylinder

$$\phi(r) \approx \left(\sigma b R_{cilium}\right)^{2/3} \left(r/b\right)^{-2/3}, \quad \text{for } r > R_{cilium}\text{, good or athermal solvent} \tag{S18}$$

Lateral distribution. The mesh size of a single cylindrical brush in its unperturbed state increases as a power law of distance r from the center of the cylinder (eq. S16 and dashed line in **fig. S3E**) due to the steric repulsion between tethered macromolecules. Such non-uniform lateral distribution of mesh sizes could lead to a non-uniform lateral distribution of probe molecules and hence their fluorescent intensity. It will be shown below that the

compression of cylindrical brushes (**fig. S3C**) due to the confinement by the neighboring cilia leads to an almost uniform lateral distribution of mesh sizes and therefore probe molecules.

The thickness of a cylindrical brush decreases under compression from its unperturbed thickness L_0 to a smaller value L, shown in **fig. S3C, D**. The volume occupied by the grafted polymers is reduced and thus the lateral polymer concentration increases (mesh size decreases). The increase of the lateral polymer concentration, however, only occurs at distance r larger than certain crossover value r_c, illustrated in **fig. S3D** and by the solid line in **fig. S3E**. In the region with distance r smaller than r_c the concentration profile is almost unperturbed following the same power law as eq. S18. The lateral concentration (mesh size) profile at distance r larger than r_c is uniform with the value on the order of $\xi(r_c)$ (eq. S18) corresponding to the unperturbed concentration of polymers at distance r_c. The crossover distance r_c is determined by the thickness L of the cylindrical brush under compression

$$\int_{r_c}^{L_0} \phi(r) 2\pi r dr = \phi(r_c) \int_{r_c}^{L} 2\pi r dr \tag{S19}$$

From the expression of $\phi(r)$ (eq. S18) one obtains the relation between the compressed brush thickness L and the crossover distance r_c

$$L^2 = \frac{1}{2} r_c^{2/3} \left(3L_0^{4/3} - r_c^{4/3} \right) \tag{S20}$$

The compression ratio defined as the ratio between the volumes occupied by the tethered polymers after and before compression

$$\Lambda \equiv \frac{L^2 - R_{cilium}^2}{L_0^2 - R_{cilium}^2} \tag{S21}$$

can be rewritten as

$$\Lambda \equiv \frac{1}{1-\left(R_{cilium}/L_0\right)^2}\left[\frac{3}{2}\left(\frac{r_c}{L_0}\right)^{2/3}-\frac{1}{2}\left(\frac{r_c}{L_0}\right)^2-\left(\frac{R_{cilium}}{L_0}\right)^2\right] \tag{S22}$$

The fraction of the volume occupied by the tethered polymers in which the mesh size has uniform lateral distribution is

$$\Gamma \equiv \frac{L^2-r_c^2}{L^2-R_{cilium}^2} \tag{S23}$$

Using eqs. S20, S22, and S23 one can estimate the lateral distribution of mesh sizes under compression. The radius of a cilium is $R_{cilium} \approx 50\,\text{nm}$. The distance between centers of two neighboring cilia is about 300 nm, corresponding to the compression thickness $L \approx 150\,\text{nm}$.The major component of tethered polymers is MUC4, with a contour length $l_{contour} \approx 1\,\mu\text{m}$ (*57*). Therefore, the average end-to-end distance *R* of an isolated MUC4 is $R \approx b\left(l_{contour}/b\right)^{3/5} \approx 150\,\text{nm}$, assuming that the Kuhn length of mucin molecules is $b \approx 10\,\text{nm}$ (*58*). The polymers (e.g., MUC4) in a cylindrical brush are extended, implying that the unperturbed brush thickness L_0 defined as the sum of cilium radius and the size of a stretched polymer is larger than $R + R_{cilium} \approx 200\,\text{nm}$. Even for L_0 = 200 nm the compression ratio defined in eq. S21 is $\Lambda \approx 0.53$, at which the crossover distance r_c= 50 nm is comparable to the cilium radius R_{cilium}. This indicates that almost 100% (Γ≈ 1) of the volume occupied by the grafted polymers has uniform lateral distribution of mesh sizes and, therefore, there is almost no lateral concentration profile in this compressed cylindrical brush. Larger values of L_0 > 200 nm result in stronger compression and thus uniform lateral distribution of mesh sizes, leading to almost uniform lateral distribution of fluorescent intensity of probe molecules.

Mesh size profile. The data from PCL-permeability experiments (solid squares in **fig. S2E**) suggests that probe molecules penetrate into the PCL further as their size decreases. Assuming that probe molecules penetrate into the PCL down to distance z from the cell surface at which the mesh size $\xi(z)$ is on the order of probe diameter d, such dependence of penetration depth on the size of probe molecules provides an indirect measurement of mesh size profile in the PCL: $\xi(z) \approx d(z)$. The determined penetration profile $d(z)$ for probe molecules of different sizes is shown by the solid line in **fig. S2E** (see eq. S14). The mesh size profile $\xi(z)$ in the PCL can be approximated by a logarithmic dependence on the distance z from the cell surface:

$$\xi(z) = d(z) \approx \bar{\xi} \log\left(\frac{z_0}{z_0 - z}\right), \quad \text{for } 0 < z < z_0 \tag{S24}$$

in which the characteristic mesh size of the PCL $\bar{\xi} \approx 16$ nm . Such decay of the mesh size towards the cell surface indicates that the tethered macromolecules form a gradient protective layer that prevents external objects from reaching the cell surface. Similarly from the mesh size profile (eq. S24) one can estimate the concentration profile of the tethered macromolecules in the PCL.

$$\phi(z) \approx b^{(3\nu-1)/\nu} \xi(z)^{(1-3\nu)/\nu} \approx \left(\frac{b}{\bar{\xi}}\right)^{4/3} \left[\log\left(\frac{z_0}{z_0 - z}\right)\right]^{-4/3}, \quad \text{for } z_{\min} < z < z_0 \tag{S25}$$

where $z_{\min}$ is the minimum distance from the cell surface at which the mesh size $\xi(z_{\min})$ of the PCL is comparable to the Kuhn length b of mucins. Considering $b \approx 10$ nm (*59*) the value of $z_{\min}$ is about 3 μm.

Cilia height under osmotic compression. The force required to bend a cilium is on the order of 50 pN (*60, 61*). Considering that the cross area per cilium is about $\pi L^2 \approx 7 \times 10^{-14}$ m^2, the required pressure to bend a cilium is on the order of 700 Pa, which is within the range of our experimental measurements (P_{cc} = 800 ± 120 Pa, see **Fig. 6E**). However, one should note that effective compression of the cilium requires the pressure difference between its top and bottom sides. The mechanism of cilia bending under high osmotic compression is the subject of our current investigation.

Supplementary Figures

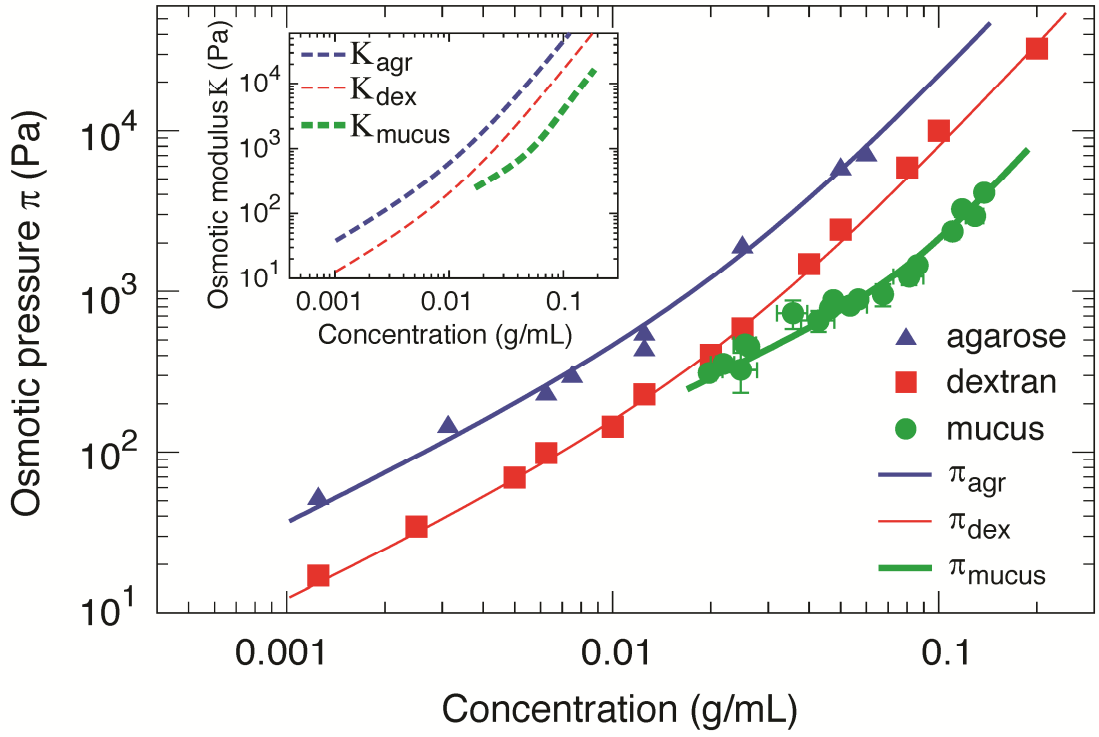

Fig. S1. Osmotic pressure and modulus of mucus simulants and native mucus. Red squares: osmotic pressure of dextran solutions in PBS at room temperature; thin solid red line corresponds to dependence of osmotic pressure on solution concentration predicted by eq. S4. Blue triangles: osmotic pressure of agarose solutions in PBS; medium solid blue line is the best fit of the concentration dependence of agarose solution osmotic pressure (eq. S8). Green circles: osmotic pressure of native mucus; thick solid green line—best fit of mucus osmotic pressure (eq. S10). Insert: thin dashed red line—calculated osmotic modulus of dextran solutions (eq. S7); medium dashed blue line—calculated osmotic modulus of agarose solution (eq. S9); thick dashed green line—calculated mucus osmotic modulus (eq. S11). Note that the concentrations of mucus are all within the physiological range.

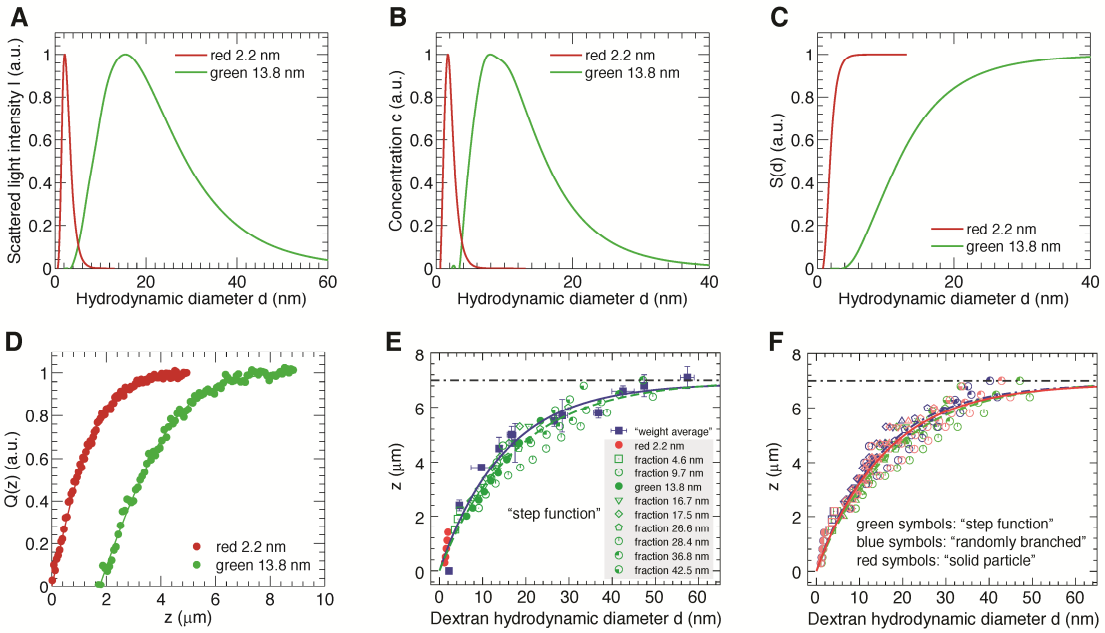

Fig. S2. Protocol and results for "profile analysis" of penetration of molecules in to the periciliary layer. (A) Typical intensity-size distribution curves of red dextran molecules (3 kDa Texas Red dextran; weight average hydrodynamic diameter $\langle d \rangle_w$ = 2.2 nm; red line) and a fraction of green dextran molecules (fraction 36 of 2 MDa stock dextran; $\langle d \rangle_w$ = 13.8 nm; green line). **(B)** Normalized concentration-size distribution curves converted from the intensity-size distribution curves in **(A)** using relation eq. S12 for 2.2 nm red dextran (red line) and 13.8 nm green dextran (green line). **(C)** Predicted normalized concentration distribution $S(d)$ of red (red line) and green probe molecules (green line) smaller than d using "step function" approximation. **(D)** Normalized measured fluorescent intensity (concentration) of red and green probe molecules within the PCL versus their distance z from the cell surface. **(E)** Dependence of distance z from the cell surface on the hydrodynamic diameter d of dextran molecules: blue solid squares—results obtained using the weight average hydrodynamic diameter of dextran fractions, solid line—best fit of these data $z(d) \approx 6.9\mu m[1-\exp(-d/15.0nm)]$; green symbols— results based on "full profile analysis" using "step function" approximation, dashed line—best fit of these data $z(d) \approx 7.0\mu m[1-\exp(-d/17.5nm)]$. Note that the red solid circles are results for 3 kDa Texas Red dextran. **(F)** Comparison between the results from the "full profile analysis" using "step function" approximation (green symbols, green dashed line—best fit of these data $z(d) \approx 7.0\mu m[1-\exp(-d/17.5nm)]$), "randomly branched" approximation assuming that dextran is a randomly branched polymer with γ = 2 in eq. S15 (blue symbols, blue dash-dotted line—best fit of these data $z(d) \approx 6.9\mu m[1-\exp(-d/15.0\ nm)]$), and "solid particle" approximation assuming that dextran molecules are solid particles with γ = 3 in eq. S15 (red symbols, red solid line—best fit of these data $z(d) \approx 6.9\mu m[1-\exp(-d/15.8\ nm)]$). Black dash-dotted lines in **(E)** and **(F)** correspond to the 7 μm length of extended cilia.

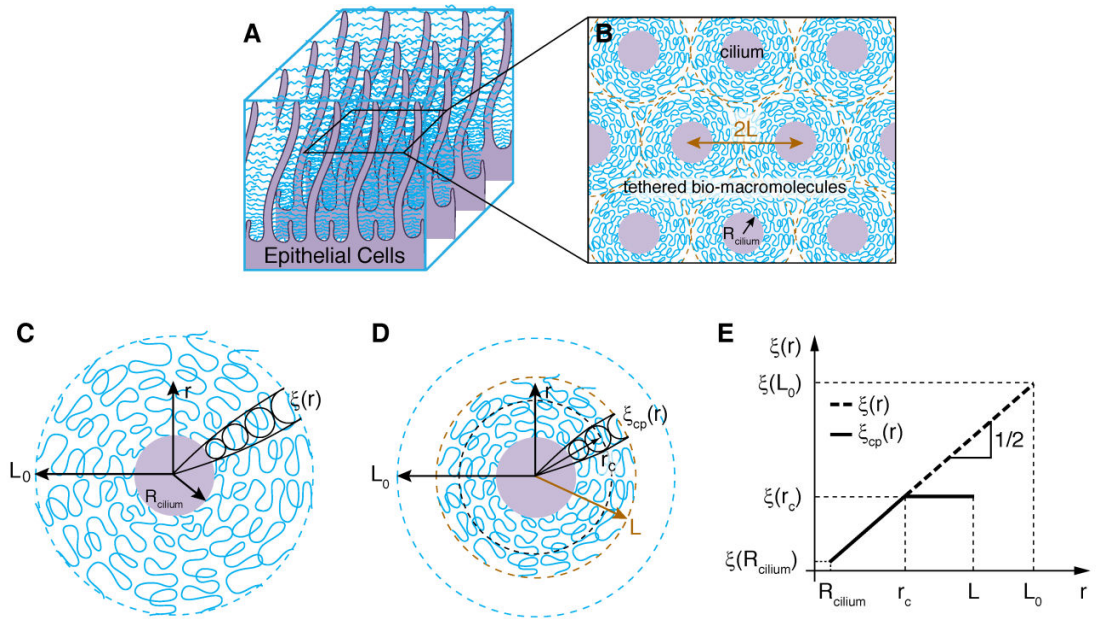

Fig. S3. Brush model of the PCL. (A) PCL is modeled as an array of cylindrical brushes; **(B)** Lateral cross-section view of the PCL as an array of cylindrical brushes, in which bio-macromolecules are tethered to the cylindrical cilia. The radius of a cilium is R_{cilium} and the distance between the centers of two neighboring cilia is $2L$. **(C)** An unperturbed single cilium brush with thickness L_0 expected to be larger than L. **(D)** The brush is compressed laterally from its unperturbed thickness L_0 to L due to the limited space between neighboring cilia. **(E)** Mesh size profile for an unperturbed cilium brush (dashed line) and a laterally compressed cilium brush (solid line). Logarithmic scales.

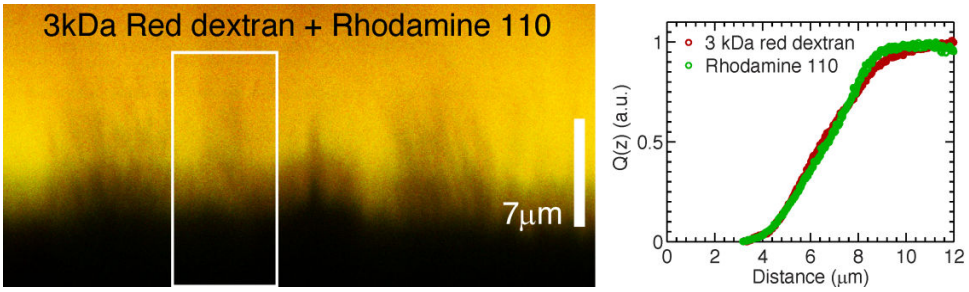

Fig. S4. Representative XZ-confocal images for HBE cells added with dilute mixture solution of unfractionated Texas Red dextran with average molecular weight 3 kDa and Rhodamine 110. Rhodamine 110 is a fluorescently green molecule of very small size (hydrodynamic diameter ~ 1.6 nm (*62*)). The overlap between the penetration for the 3 kDa red dextran and that for green Rhodamine 110 into the PCL, shown by the yellow zone, suggests that the 3 kDa red dextran can also reach the cell surface. This is further demonstrated by the overlap of the normalized intensity profiles for both the red dextran and green Rhodamine molecules.

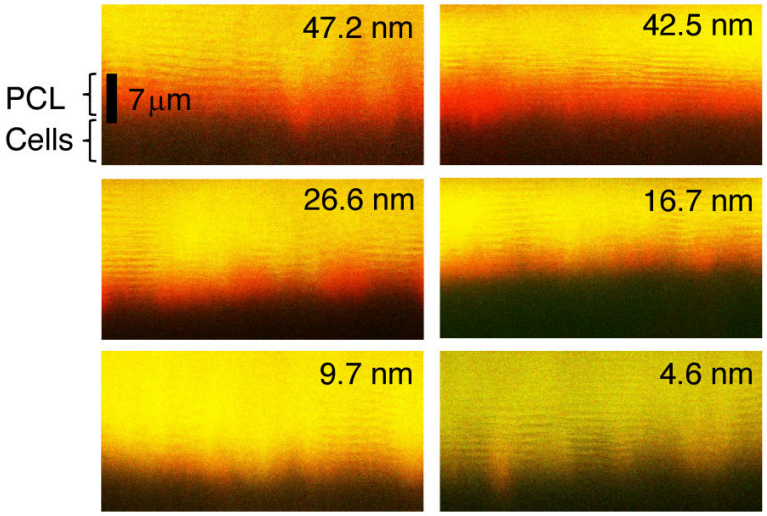

$\langle d \rangle_w$ (nm)	z_{PCL} (μm)
47.4±0.5	6.8±0.4
42.4±2.6	6.6±0.2
26.6±0.5	5.5±0.2
16.7±1.0	5.0±0.3
9.7±2.4	3.8±0.1
4.6±0.8	2.4±0.2

Fig. S5. Representative confocal images showing the exclusion thickness z_{PCL} of probe molecules of different sizes in the PCL. The table shows the exact numbers of weight average hydrodynamic diameter $\langle d \rangle_w$ and the corresponding exclusion thicknesses z_{PCL}.

Supplementary Tables

Table S1. List of fitting parameters z_0 and $\bar{\xi}$ of eq. S14 to results from different analyses.

		Full profile analysis		
	Weight average	Step function	Randomly branched	Solid particle
z_0 (μm)	6.9±0.8	7.0±0.5	6.9±0.4	6.9±0.4
$\bar{\xi}$ (nm)	15.0±3.7	17.5±2.4	15.0±2.0	15.8±2.1

References and Notes

1. J. V. Fahy, B. F. Dickey, Airway mucus function and dysfunction. *N. Engl. J. Med.* **363**, 2233 (2010). doi:10.1056/NEJMra0910061 Medline

2. P. M. Quinton, Physiological basis of cystic fibrosis: A historical perspective. *Physiol. Rev.* **79** (suppl.), S3 (1999). Medline

3. J. J. Wine, N. S. Joo, Submucosal glands and airway defense. *Proc. Am. Thorac. Soc.* **1**, 47 (2004). doi:10.1513/pats.2306015 Medline

4. M. Kaliner, Z. Marom, C. Patow, J. Shelhamer, Human respiratory mucus. *J. Allergy Clin. Immunol.* **73**, 318 (1984). doi:10.1016/0091-6749(84)90403-2 Medline

5. M. R. Knowles, R. C. Boucher, Mucus clearance as a primary innate defense mechanism for mammalian airways. *J. Clin. Investig.* **109**, 571 (2002). Medline

6. J. C. Hogg *et al*., The nature of small-airway obstruction in chronic obstructive pulmonary disease. *N. Engl. J. Med.* **350**, 2645 (2004). doi:10.1056/NEJMoa032158 Medline

7. R. C. Boucher, Airway surface dehydration in cystic fibrosis: Pathogenesis and therapy. *Annu. Rev. Med.* **58**, 157 (2007). doi:10.1146/annurev.med.58.071905.105316 Medline

8. R. Tarran *et al*., The CF salt controversy: In vivo observations and therapeutic approaches. *Mol. Cell* **8**, 149 (2001). doi:10.1016/S1097-2765(01)00286-6 Medline

9. L. A. Clunes *et al*., Cigarette smoke exposure induces CFTR internalization and insolubility, leading to airway surface liquid dehydration. *FASEB J.* **26**, 533 (2012). doi:10.1096/fj.11-192377 Medline

10. R. Tarran, Regulation of airway surface liquid volume and mucus transport by active ion transport. *Proc. Am. Thorac. Soc.* **1**, 42 (2004). doi:10.1513/pats.2306014 Medline

11. M. Mall, B. R. Grubb, J. R. Harkema, W. K. O'Neal, R. C. Boucher, Increased airway epithelial Na+ absorption produces cystic fibrosis-like lung disease in mice. *Nat. Med.* **10**, 487 (2004). doi:10.1038/nm1028 Medline

12. H. Matsui *et al*., A physical linkage between cystic fibrosis airway surface dehydration and *Pseudomonas aeruginosa* biofilms. *Proc. Natl. Acad. Sci. U.S.A.* **103**, 18131 (2006). doi:10.1073/pnas.0606428103 Medline

13. R. C. Boucher, New concepts of the pathogenesis of cystic fibrosis lung disease. *Eur. Respir. J.* **23**, 146 (2004). doi:10.1183/09031936.03.00057003 Medline

14. A. Wanner, M. Salathé, T. G. O'Riordan, Mucociliary clearance in the airways. *Am. J. Respir. Crit. Care Med.* **154**, 1868 (1996). Medline

15. A. M. Lucas, L. C. Douglas, Principles underlying ciliary activity in the respiratory tract: II. A comparison of nasal clearance in man, monkey and other mammals. *Arch. Otolaryngol.* **20**, 518 (1934). doi:10.1001/archotol.1934.03600040074006

16. E. Houtmeyers, R. Gosselink, G. Gayan-Ramirez, M. Decramer, Regulation of mucociliary clearance in health and disease. *Eur. Respir. J.* **13**, 1177 (1999). doi:10.1034/j.1399-3003.1999.13e39.x Medline

17. H. Kalhoff, Mild dehydration: A risk factor of broncho-pulmonary disorders? *Eur. J. Clin. Nutr.* **57** (suppl. 2), S81 (2003). doi:10.1038/sj.ejcn.1601906 Medline

18. D. J. Smith, E. A. Gaffney, J. R. Blake, A model of tracer transport in airway surface liquid. *Bull. Math. Biol.* **69**, 817 (2007). doi:10.1007/s11538-006-9163-z Medline

19. J. Iravani, A. Van As, Mucus transport in the tracheobronchial tree of normal and bronchitic rats. *J. Pathol.* **106**, 81 (1972). doi:10.1002/path.1711060204 Medline

20. A. C. Hilding, The role of the respiratory mucosa in health and disease. *Minn. Med.* **50**, 915 (1967). Medline

21. M. C. Rose, Mucins: Structure, function, and role in pulmonary diseases. *Am. J. Physiol.* **263**, L413 (1992). Medline

22. C. Wickström, J. R. Davies, G. V. Eriksen, E. C. I. Veerman, I. Carlstedt, MUC5B is a major gel-forming, oligomeric mucin from human salivary gland, respiratory tract and endocervix: Identification of glycoforms and C-terminal cleavage. *Biochem. J.* **334**, 685 (1998). Medline

23. D. J. Thornton, K. Rousseau, M. A. McGuckin, Structure and function of the polymeric mucins in airways mucus. *Annu. Rev. Physiol.* **70**, 459 (2008). doi:10.1146/annurev.physiol.70.113006.100702 Medline

24. M. Kesimer, A. M. Makhov, J. D. Griffith, P. Verdugo, J. K. Sheehan, Unpacking a gel-forming mucin: a view of MUC5B organization after granular release. *Am. J. Physiol. Lung Cell. Mol. Physiol.* **298**, L15 (2010). doi:10.1152/ajplung.00194.2009 Medline

25. H. W. Hovenberg, J. R. Davies, I. Carlstedt, Different mucins are produced by the surface epithelium and the submucosa in human trachea: Identification of MUC5AC as a major mucin from the goblet cells. *Biochem. J.* **318**, 319 (1996). Medline

26. J. K. Sheehan *et al*., Physical characterization of the MUC5AC mucin: A highly oligomeric glycoprotein whether isolated from cell culture or in vivo from respiratory mucous secretions. *Biochem. J.* **347**, 37 (2000). doi:10.1042/0264-6021:3470037 Medline

27. B. D. Raynal, T. E. Hardingham, D. J. Thornton, J. K. Sheehan, Concentrated solutions of salivary MUC5B mucin do not replicate the gel-forming properties of saliva. *Biochem. J.* **362**, 289 (2002). doi:10.1042/0264-6021:3620289 Medline

28. J. H. Widdicombe, J. G. Widdicombe, Regulation of human airway surface liquid. *Respir. Physiol.* **99**, 3 (1995). doi:10.1016/0034-5687(94)00095-H Medline

29. C. L. Hattrup, S. J. Gendler, Structure and function of the cell surface (tethered) mucins. *Annu. Rev. Physiol.* **70**, 431 (2008). doi:10.1146/annurev.physiol.70.113006.100659 Medline

30. W. E. Finkbeiner *et al*., Cystic fibrosis and the relationship between mucin and chloride secretion by cultures of human airway gland mucous cells. *Am. J. Physiol. Lung Cell. Mol. Physiol.* **301**, L402 (2011). doi:10.1152/ajplung.00210.2010 Medline

31. M. E. Monzon, S. M. Casalino-Matsuda, R. M. Forteza, Identification of glycosaminoglycans in human airway secretions. *Am. J. Respir. Cell Mol. Biol.* **34**, 135 (2006). doi:10.1165/rcmb.2005-0256OC Medline

32. M. Rubinstein, R. H. Colby, *Polymer Physics* (Oxford Univ. Press, Oxford, 2003).

33. G. B. Arfken, H. J. Weber, *Mathematical Methods for Physicists* (Elsevier, Boston, ed. 6, 2005).

34. R. Tarran, B. R. Grubb, J. T. Gatzy, C. W. Davis, R. C. Boucher, The relative roles of passive surface forces and active ion transport in the modulation of airway surface liquid volume and composition. *J. Gen. Physiol.* **118**, 223 (2001). doi:10.1085/jgp.118.2.223 Medline

35. A. J. Zuckerman, J. E. Banatvala, J. R. Pattison, *Principles and Practice of Clinical Virology* (Wiley, Chichester, UK, ed. 4, 2000).

36. S. K. Lai, Y. Y. Wang, J. Hanes, Mucus-penetrating nanoparticles for drug and gene delivery to mucosal tissues. *Adv. Drug Deliv. Rev.* **61**, 158 (2009). doi:10.1016/j.addr.2008.11.002 Medline

37. M. P. Kinsky, S. M. Milner, B. Button, M. A. Dubick, G. C. Kramer, Resuscitation of severe thermal injury with hypertonic saline dextran: Effects on peripheral and visceral edema in sheep. *J. Trauma Inj. Infect. Crit. Care* **49**, 844 (2000). doi:10.1097/00005373-200011000-00009

38. Materials and methods are available as supplementary materials on *Science* Online.

39. L. W. Matthews, S. Spector, J. Lemm, J. L. Potter, Studies on pulmonary secretions. I. The over-all chemical composition of pulmonary secretions from patients with cystic fibrosis, bronchiectasis, and laryngectomy. *Am. Rev. Respir. Dis.* **88**, 199 (1963). Medline

40. R. S. Baltimore, C. D. Christie, G. J. Smith, Immunohistopathologic localization of Pseudomonas aeruginosa in lungs from patients with cystic fibrosis. Implications for the pathogenesis of progressive lung deterioration. *Am. Rev. Respir. Dis.* **140**, 1650 (1989). doi:10.1164/ajrccm/140.6.1650 Medline

41. D. Worlitzsch *et al*., Effects of reduced mucus oxygen concentration in airway *Pseudomonas* infections of cystic fibrosis patients. *J. Clin. Investig.* **109**, 317 (2002). Medline

42. U. Schwab *et al*., Patterns of epithelial cell invasion by different species of the *Burkholderia cepacia* complex in well-differentiated human airway epithelia. *Infect. Immun.* **70**, 4547 (2002). doi:10.1128/IAI.70.8.4547-4555.2002 Medline

43. B. Jachimska, M. Wasilewska, Z. Adamczyk, Characterization of globular protein solutions by dynamic light scattering, electrophoretic mobility, and viscosity measurements. *Langmuir* **24**, 6866 (2008). doi:10.1021/la800548p Medline

44. S. K. Lai *et al*., Rapid transport of large polymeric nanoparticles in fresh undiluted human mucus. *Proc. Natl. Acad. Sci. U.S.A.* **104**, 1482 (2007). doi:10.1073/pnas.0608611104 Medline

45. B. C. Tang *et al*., Biodegradable polymer nanoparticles that rapidly penetrate the human mucus barrier. *Proc. Natl. Acad. Sci. U.S.A.* **106**, 19268 (2009). doi:10.1073/pnas.0905998106 Medline

46. J. H. Raphael, D. A. Selwyn, S. D. Mottram, J. A. Langton, C. O. O'Callaghan, Effects of 3 MAC of halothane, enflurane and isoflurane on cilia beat frequency of human nasal epithelium in vitro. *Br. J. Anaesth.* **76**, 116 (1996). doi:10.1093/bja/76.1.116 Medline

47. N. O. Chahine, F. H. Chen, C. T. Hung, G. A. Ateshian, Direct measurement of osmotic pressure of glycosaminoglycan solutions by membrane osmometry at room temperature. *Biophys. J.* **89**, 1543 (2005). doi:10.1529/biophysj.104.057315 Medline

48. M. L. Fulcher, S. Gabriel, K. A. Burns, J. R. Yankaskas, S. H. Randell, Well-differentiated human airway epithelial cell cultures. *Methods Mol. Med.* **107**, 183 (2005). Medline

49. A. P. Corfield, D. Carroll, N. Myerscough, C. S. Probert, Mucins in the gastrointestinal tract in health and disease. *Front. Biosci.* **6**, D1321 (2001). doi:10.2741/Corfield Medline

50. S. Singh, K. C. Khulbe, T. Matsuura, P. Ramamurthy, Membrane characterization by solute transport and atomic force microscopy. *J. Membr. Sci.* **142**, 111 (1998). doi:10.1016/S0376-7388(97)00329-3

51. R. Tarran, R. C. Boucher, Thin-film measurements of airway surface liquid volume/composition and mucus transport rates in vitro. *Methods Mol. Med.* **70**, 479 (2002). Medline

52. J. A. M. Smit, J. A. P. P. Vandijk, M. G. Mennen, M. Daoud, Polymer size exponents of branched dextrans. *Macromolecules* **25**, 3585 (1992). doi:10.1021/ma00039a044

53. M. Daoud, J. F. Joanny, Conformation of branched polymers. *J. Phys. (Paris)* **42**, 1359 (1981). doi:10.1051/jphys:0198100420100135900

54. J. Isaacson, T. C. Lubensky, Flory exponents for generalized polymer problems. *J. Phys. Lett. (Paris)* **41**, 469 (1980). doi:10.1051/jphyslet:019800041019046900

55. P. G. de Gennes, Conformations of polymers attached to an interface. *Macromolecules* **13**, 1069 (1980). doi:10.1021/ma60077a009

56. C. M. Wijmans, E. B. Zhulina, Polymer brushes at curved surfaces. *Macromolecules* **26**, 7214 (1993). doi:10.1021/ma00078a016

57. N. Moniaux *et al*., Complete sequence of the human mucin MUC4: A putative cell membrane-associated mucin. *Biochem. J.* **338**, 325 (1999). doi:10.1042/0264-6021:3380325 Medline

58. N. Jentoft, Why are proteins O-glycosylated? *Trends Biochem. Sci.* **15**, 291 (1990). doi:10.1016/0968-0004(90)90014-3 Medline

59. R. Bansil, E. Stanley, J. T. LaMont, Mucin biophysics. *Annu. Rev. Physiol.* **57**, 635 (1995). doi:10.1146/annurev.ph.57.030195.003223 Medline

60. M. Okuno, Y. Hiramoto, *J. Exp. Biol.* **79**, 235 (1979).

61. D. B. Hill *et al*., Force generation and dynamics of individual cilia under external loading. *Biophys. J.* **98**, 57 (2010). doi:10.1016/j.bpj.2009.09.048 Medline

62. D. Pristinski, V. Kozlovskaya, S. A. Sukhishvili, Fluorescence correlation spectroscopy studies of diffusion of a weak polyelectrolyte in aqueous solutions. *J. Chem. Phys.* **122**, 14907 (2005). doi:10.1063/1.1829255 Medline